Nuclear Instruments and Methods in Physics Research A290 (1990) 95–108
North-Holland

RESPONSE OF A URANIUM–SCINTILLATOR CALORIMETER TO ELECTRONS, PIONS AND PROTONS IN THE MOMENTUM RANGE 0.5–10 GeV/c

The ZEUS Calorimeter Group
A. ANDRESEN [1], A. BAMBERGER [2], U. BEHRENS [3], J. CRITTENDEN [4], A. CALDWELL [5], J. DAWSON [6], J. ENGELEN [7], B. FRISKEN [10], D. GILKINSON [8], R. HAMATSU [9], D. HANNA [8], D. HASELL [10], L. HERVAS [11], U. HOLM [3], A. FÜRTJES [12], R. KLANNER [12], P. KOOIJMAN [7], U. KÖTZ [12], M. KRÄMER [4], J. KRÜGER [1], G. LEVMAN [13], P. MALECKI [12], J. MARTIN [13], J. MITCHELL [8], P. PATEL [8], M. ROHDE [12], T. ROMANOWSKI [14], E. ROS [12], W. SIPPACH [5], D. SCHÄCKE [2], J. STRAVER [7], H. TIECKE [7], T. TSURUGAI [1], W. VOGEL [12], K. WICK [3] and C. YOUNGMAN [1]

[1] *Universität Hamburg, II Inst., 2000 Hamburg 13, FRG* *
[2] *Albert-Ludwigs-Universität, 7800 Freiburg FRG* *
[3] *Universität Hamburg, I Inst., 2000 Hamburg 13, FRG* *
[4] *Rheinische Friedrich-Wilhelms-Universität, 5300 Bonn, FRG* *
[5] *Columbia University, New York, NY 10027, USA* **
[6] *Argonne National Laboratory, Argonne, IL 60439, USA* §
[7] *NIKHEF-H, 1009 DB Amsterdam, The Netherlands*
[8] *McGill University, Montreal, Que., Canada H3A 2T5* §§
[9] *Tokyo Metropolitan University, 1-1-1 Yagumo, Meguro-ku, Tokyo 125, Japan*
[10] *York University, North York, Ont., Canada M3J 1P3* §§
[11] *Universidad Autónoma de Madrid, 28049 Madrid, Spain* +
[12] *DESY, 2000 Hamburg 52, FRG*
[13] *University of Toronto, Toronto, Ont., Canada M5S 1A1* §§
[14] *Ohio State University, Columbus, OH 43210, USA* §

Received 27 November 1989

We have exposed a sandwich calorimeter, consisting of 3.3 mm thick uranium plates interleaved with 2.6 mm thick scintillator tiles, to positive and negative electrons and pions and to protons in the momentum range of 0.5 to 10 GeV/c. We find that e/h is about 1 above 3 GeV/c, but decreases significantly for lower momenta. This ratio is the same for positive and negative pions and also for pions and protons of the same kinetic energy.

1. Introduction

The ZEUS Collaboration [1] is presently constructing a uranium–scintillator calorimeter as the central component for a detector at the high energy electron–proton collider HERA. It has been shown experimentally [2,3] that uranium–scintillator calorimeters achieve compensation (equal response to electrons and hadrons) for a correct choice of the absorber-to-readout material thickness ratio [4] and an energy resolution for hadrons of $35\%/\sqrt{E}$. Four prototype modules were constructed and tested up to beam momenta of 100 GeV/c [5], and the requirements on uniformity and calibration to achieve the desired performance were studied in detail. In this article we report measurements performed with electrons, pions and protons, with emphasis on the calorimeter response to low-momentum particles, around 1 Gev/c. The aim of these measurements was to understand the response of the ZEUS calorimeter to the low-energy component of jets and also to provide data which could be used to check the predictions of hadron shower Monte Carlo programs. Similar measurements performed by the R807 Collaboration have been presented in ref. [2].

* Supported by BMFT.
** Supported by NSF.
§ Supported by DOE.
§§ Supported by NSERC.
+ Supported by CAICYT.

0168-9002/90/$03.50 © 1990 – Elsevier Science Publishers B.V. (North-Holland)

2. Description of the calorimeter

The calorimeter consisted of four identical modules. They were constructed as prototype modules for the ZEUS forward calorimeter following the same mechanical design as the final modules, except for a reduced height. Each module consisted of four 20×20 cm^2 towers and was segmented longitudinally into an electromagnetic part (EMC, 1 λ thick) and two hadronic sections (HAC1 and HAC2, each 3 λ thick). The EMC part was further segmented into four 5×20 cm^2 sections in the transverse direction.

The sandwich structure of the calorimeter consisted of 3.3 mm thick depleted uranium plates (DU) interleaved with 2.6 mm thick scintillator tiles (SCI) of the SCSN-38 type. The DU plates were clad with 0.2 and 0.4 mm of stainless steel in the EMC and HAC sections, respectively. The SCI tiles were wrapped in Tyvek paper with a printed black pattern, to achieve a good readout uniformity. The first EMC layer was an aluminum plate, 15 mm thick, followed by a SCI plate and 25 DU-SCI layers. After DU plates 3 and 6, a 10 mm deep gap was instrumented with arrays of 10 cm^2 silicon diode detectors in order to improve the electron-hadron separation. Each of the two HAC sections consisted of 80 DU-SCI layers. The total thickness of a DU-SCI layer was 7.6 mm in the EMC and 8.0 mm in the HAC. In order to avoid any pressure on the scintillator, the DU plates were kept at distance by tungsten-carbide spacers located at the corners of the 20×20 cm^2 towers. Their cross-section was 5×6 mm^2 in the EMC and 5×10 mm^2 in the HAC.

Each section was read out on the left and right side by the wavelength shifter plates (WLS), light guides (LG) and photomultipliers (PM). The WLS plates were 2 mm thick and consisted of PMMA doped with Y7 in a concentration of 45 ppm or 30 ppm for EMC or HAC sections, respectively. The uniformity of the WLS response was achieved with end and back reflectors. The PMs were of the type XP2972 and XP2081 from Valvo for EMC and HAC sections, respectively.

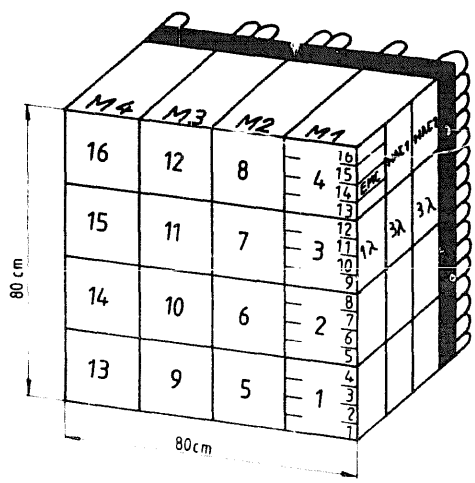

Fig. 1. View of the calorimeter arrangement in the test beam area, showing module, tower and section numbering.

Table 1
Main calorimeter parameters

	EMC	HAC
Absorber material	Depleted uranium (DU)	
Absorber cladding	stainless steel	
Readout material	SCSN-38 scintillator (SCI)	
DU thickness [mm]	3.3	3.3
Cladding thickness [mm]	0.2	0.4
SCI thickness [mm]	2.6	2.6
Effective X_0 [mm]	7.4	7.6
Effective λ [mm]	210	207
Effective R_M [mm]	20.2	20.0
Effective density [g/cm^3]	8.7	8.7
Transverse segmentation	5×20 cm^2	20×20 cm^2
Longitudinal Segmentation	$25.9 X_0$ (0.96λ)	HAC1 (3.09λ) HAC2 (3.09λ)
Total length [cm]	24.1	128.0
Total cross-section	80×80 cm^2	80×80 cm^2
Optical readout	2 mm thick WLS plates + light guides	
WLS material	PMMA + Y7 (45 ppm)	PMMA + Y7 (30 ppm)
Photomultipliers	XP2972 (Valvo)	XP2081 (Valvo)
Number of readout channels	128	64

These four modules formed a calorimeter of 80×80 cm^2 cross-section and 7λ thickness (see fig. 1). The main calorimeter parameters are summarized in table 1. More details about the mechanical structure of the calorimeter can be found in ref. [5].

3. Experimental setup

The measurements were performed in the T7 beam of the CERN-PS. The experimental setup is shown in fig. 2. It consisted of four scintillation counters (B1 to B4) to define the beam and two Cherenkov counters (C1 and C2) for particle identification. The dimensions of the B1 and B2 counters were 10×10 cm^2 and B3 was a 80×80 cm^2 veto counter, with a 3 cm diameter hole in the centre, used to reject beam halo particles. The B4 counter, located behind the calorimeter, was used to trigger on muons. Both Cherenkov counters were filled with CO_2 and two pressure values were used: the first, pr_1, was optimized for electron-pion separation and the second, pr_2, for pion-proton separation (see section 6).

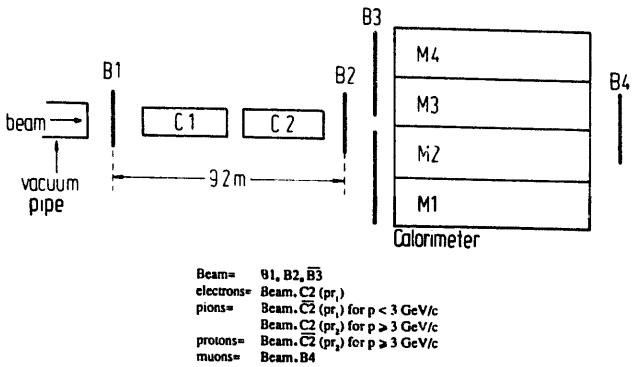

Fig. 2. Experimental setup in the beamline and trigger conditions.

Typical trigger conditions are also indicated in fig. 2. The time of flight (TOF) of beam particles between the counters B1 and B2 was measured by a TDC. Since the distance between these counters was 9.2 m, it was possible to separate protons from pions up to momenta of 2.5 GeV/c (see section 6).

In evaluating the response of the calorimeter to low-energy particles the materials in front of it traversed by beam particles must be taken into account. These materials consisted of: the window of the vacuum pipe, the front and back windows of the two Cherenkov counters, about 1.5 cm of scintillator, about 5 m of air and about 8 m of CO_2 inside the Cherenkov counters (the pressure used at low momenta was 0.8 atm). We estimate the dE/dx losses of minimum ionizing particles (mips) before reaching the calorimeter to be about 8 MeV.

4. Electronics

The electronics used in this test was similar to the final electronics of the ZEUS calorimeter and has already been described in detail in refs. [1] and [6]. The main elements are summarized below.

The PM signals were connected to (see fig. 3a):

- a dc coupled integrator used to measure the current induced by the uranium natural radioactivity (UNO signal),

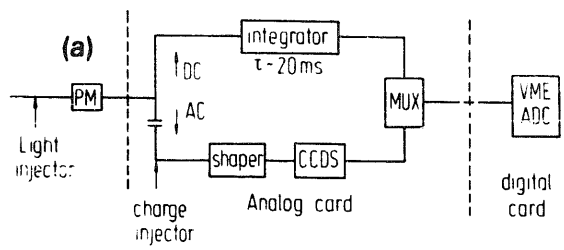

Fig. 3a. Readout electronics.

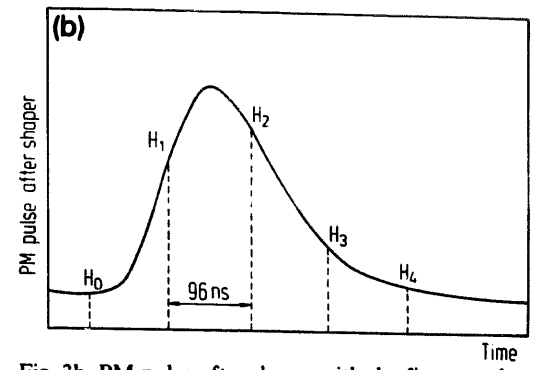

Fig. 3b. PM pulse after shaper with the five samples.

- an ac coupled shaper whose output was sampled five times every 96 ns, corresponding to the frequency of the HERA bunch crossing (see fig. 3b). The samples were pipelined by LeCroy MVV200 CCDs *.

Integrators, shapers and CCDs were mounted on front end cards (analog cards) containing 12 channels each. These analog cards, installed just behind the calorimeter, were connected to the PMs by 2 m long cables. Both the UNO signals and the pulse samples were multiplexed and digitized by 12-bit VME ADCs (digital cards) connected to the analog cards via 40 m flat twisted-pair cables. The ADCs were read out by a computer based on a Motorola 68020 microprocessor. The total number of readout channels was only 144 since the readout electronics for module 4 was not available.

The five pulse samples, H_0 to H_4, were used to reconstruct the charge deposited in each calorimeter channel and also the time of the signal. The time $t = 0$ was defined as the time at which $H_1 = H_2$. At HERA the readout will be synchronized with the beam crossing so all events arrive at $t = 0$. This was of course not possible during the test since events arrived randomly in time relative to the CCD sampling clock. The charge reconstruction used the quantity

$$H = (H_1 - H_0) + C(H_2 - H_0),$$

$$\text{with} \quad C = -\frac{(dH/dt)_1}{(dH/dt)_2}.$$

The constant C is the ratio of slopes at the position of samples 1 and 2 for events arriving at $t = 0$. The quantity H defined in this way is insensitive to small time variations around $t = 0$. In fact, only two samples, H_1 and H_2, were used to reconstruct the charge. The first sample, H_0, was used as a pedestal, and the last two samples, H_3 and H_4 were used for pulse-shape and pileup studies. The reconstructed charge Q was a non-linear function f of H since the response of the CCDs

* The CCDs will be replaced by a switched capacitor delay line in the final version of the electronics.

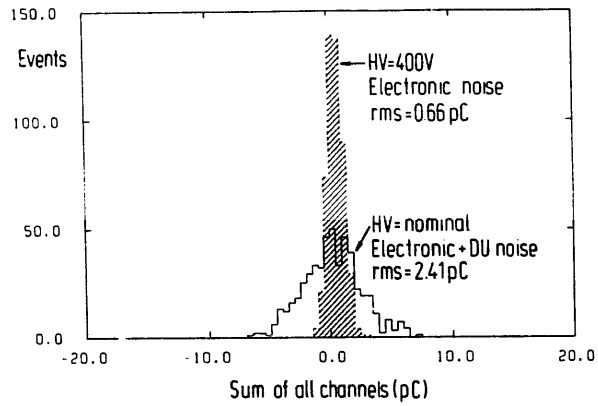

Fig. 4. Sum of all calorimeters channels for random triggers with the HV at 400 V (showing only electronic noise) and at nominal value (showing electronic and uranium noise).

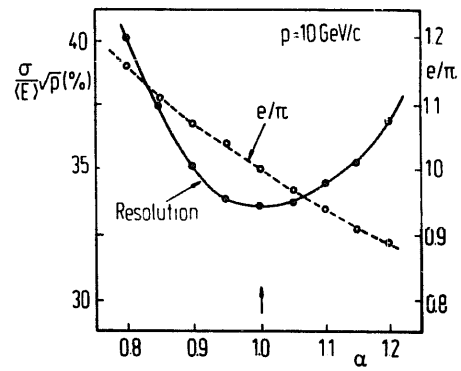

Fig. 5. Energy resolution for 10 GeV/c pions and e/h as a function of the intercalibration parameter α.

was nonlinear. The function f was determined by charge injection at the input of the shaper (see fig. 3a) and was used to correct H and the individual samples:

$$Q = f(H) \quad \text{and} \quad Q_i = f(H_i - H_0) \quad (i = 1, \cdots, 4).$$

The time T was reconstructed from the first sample and Q:

$$T = \tau(Q_1 - C_1 Q)/Q.$$

The constant C_1 was adjusted so that $T = 0$ for $t = 0$ and τ was used to adjust the time scale. The constants C, C_1 and τ were obtained from charge injection runs.

The formulae described before for Q and T are valid only for events around $t = 0$. Therefore an additional correction was performed, depending on the real time of the event. The real time, t, was measured by a TDC started by the beam trigger and stopped by the CCD sampling clock.

The total calorimeter rms noise (144 channels) was measured with random triggers and amounted to 2.41 pC (150 MeV electron equivalent energy). This noise is dominated by the fluctuations of the uranium radioactivity. The electronic noise was measured to be 0.66 pC (40 MeV) as shown in fig. 4.

5. Calibration

The calibration of the calorimeter channels was achieved with the help of:

- charge injection measurements performed every 24 h,
- uranium radioactivity measurements performed every 8 h,
- an electron calibration cycle performed at the beginning of the test.

The aim of the charge injection runs was to correct for the nonlinearities in the response of the CCDs, to calibrate the pipeline part of the readout and finally to determine the constants C, C_1 and τ introduced in the previous section.

The calibration of the EMC channels was obtained from a scan with the 5 GeV/c electron beam incident at the centre of all EMC sections. It was shown in ref. [5] that the current induced by the uranium natural radioactivity (UNO signal measured via integrators) can be used to trace PM gain variations within 1% and therefore keep the quality of the initial electron calibration during all the test. It was also shown that the UNO signal also provides a relative calibration of the HAC channels with 1% precision.

The intercalibration between EMC and HAC channels was obtained by choosing the intercalibration parameter α defined by

$$E = E_{\mathrm{EMC}} + \alpha E_{\mathrm{HAC}},$$

which gives $e/\pi = 1$ for $p = 10$ GeV/c. The value of α obtained in this way provides also an optimum fractional energy resolution for hadrons (see fig. 5). It was shown in [5] that e/π is independent of momentum at

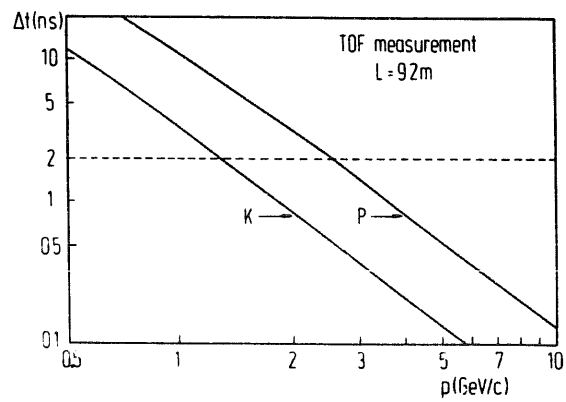

Fig. 6. TOF measured between the beam counters B1 and B2. The figure shows the difference in TOF between hadrons (protons or kaons) and pions. The limit to resolve the hadron peak from the pion peak is 2 ns.

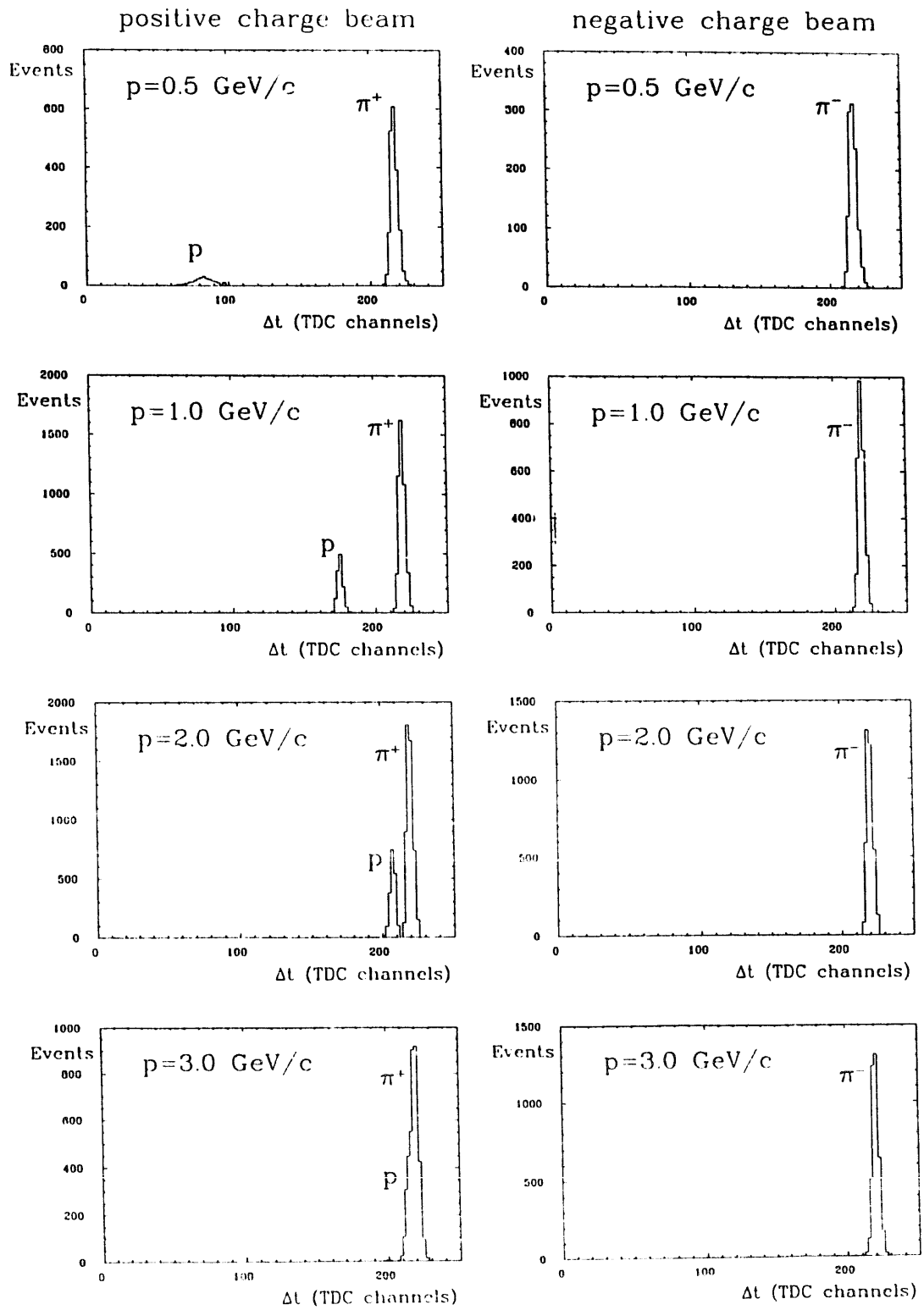

Fig. 7. TOF spectra for various beam momenta and both beam polarities.

the level of 1% in the range 10–100 GeV/c, as expected for a compensating calorimeter.

6. Particle identification

Particle identification was provided by the time-of-flight measurement, the Cherenkov counters and the calorimeter itself.

The TOF measurement was performed with the scintillation counters B1 and B2, separated by a distance L of 9.2 m as explained in section 3. The TOF difference between hadrons and pions is

$$\Delta t = \frac{L}{c}\left(\sqrt{1+\frac{m_h^2}{p^2}} - \sqrt{1+\frac{m_\pi^2}{p^2}}\right),$$

where m_h, m_π and p are the hadron mass, the pion mass and the beam momentum. The quantity Δt is plotted for kaons and protons versus p in fig. 6. The Δt spectra are displayed for beam momenta of 0.5, 1, 2, and 3 GeV/c and for both beam polarities in fig. 7. We observe that the TOF measurement had a resolution of about 0.5 ns and therefore provided a clear proton-to-pion separation up to 2.5 GeV/c. As seen in fig. 7, the proton and the pion peaks cannot be resolved at 3 GeV/c. We see no evidence for antiprotons in the beam, up to 3 GeV/c.

The pressure of the two Cherenkov counters was set for each beam momentum at two values, pr_1 and pr_2, optimized for electron-to-hadron and pion-to-proton separation, respectively. These pressure values are plotted versus beam momentum in fig. 8. The threshold pressure is

$$pr_{th} = pr_0\left(\frac{m_h}{p}\right)^2 \quad (p \gg m_h),$$

where $pr_0 = 1220$ atm for CO_2, as indicated in fig. 8 for muons, pions, kaons and protons. As the maximum allowed pressure was 4 atm, no kaon–proton separation

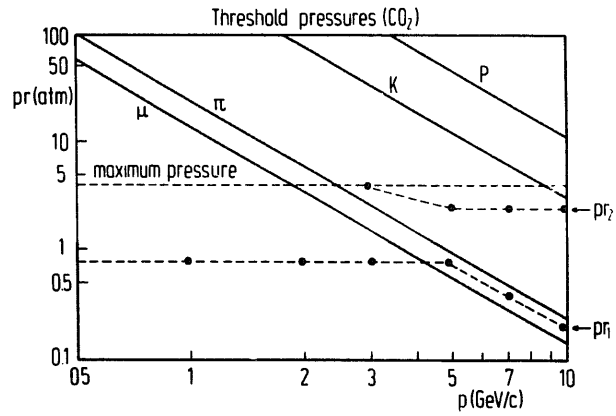

Fig. 8. Threshold pressures for muons, pions, kaons and protons in CO_2 as a function of the particle momentum. The pressures pr_1 and pr_2 used for particle identification are indicated.

was possible. The two Cherenkov counters were filled with CO_2 at the same pressure, and therefore it was possible to check their relative efficiencies which are reported in table 2 for the different beam momenta. The Cherenkov counters provided a clear electron-to-hadron separation except at the highest momentum.

The calorimeter itself provided a clear electron-to-hadron separation for $p \geq 3$ GeV/c. We defined the quantity

$$\Delta_{cal} = (E_{cal} - E_{emc})/p,$$

where E_{cal} and E_{emc} are, respectively, the total calorimeter signal and the signal measured in the EMC section where the beam was incident. The Δ_{cal} spectra are displayed in fig. 9 for various beam momenta. Hadrons were selected by the cut $\Delta_{cal} > \Delta_{cut}$. The Δ_{cut} values, the electron rejection achieved with this cut, $r_{cal}(e)$, and the hadron efficiency, $\epsilon_{cal}(h)$, are reported in table 3 for the different beam momenta.

By combining the information of the TOF, the Cherenkov counters and the calorimeter signals, pure samples of electrons, pions and protons were isolated

Table 2
Efficiency of the Cherenkov counters C1 and C2 for the two pressure values pr_1 and pr_2. The efficiency for electrons is given for pr_1 and the efficiency for hadrons for pr_2

p [GeV/c]	pr_1 [atm]	pr_2 [atm]	ϵ_1 (pr_1) [%]	ϵ_2 (pr_1) [%]	ϵ_1 (pr_2) [%]	ϵ_2 (pr_2) [%]
0.50	0.8	–	80	95	–	–
0.75	0.8	–	77	96	–	–
1.00	0.8	–	77	97	–	–
1.50	0.8	–	77	97	–	–
2.00	0.8	–	78	97	–	–
3.00	0.8	3.9	79	96	96	99
5.00	0.8	2.5	72	91	96	99
7.00	0.4	2.5	71	67	98	99
10.00	0.2	2.5	25	17	98	98

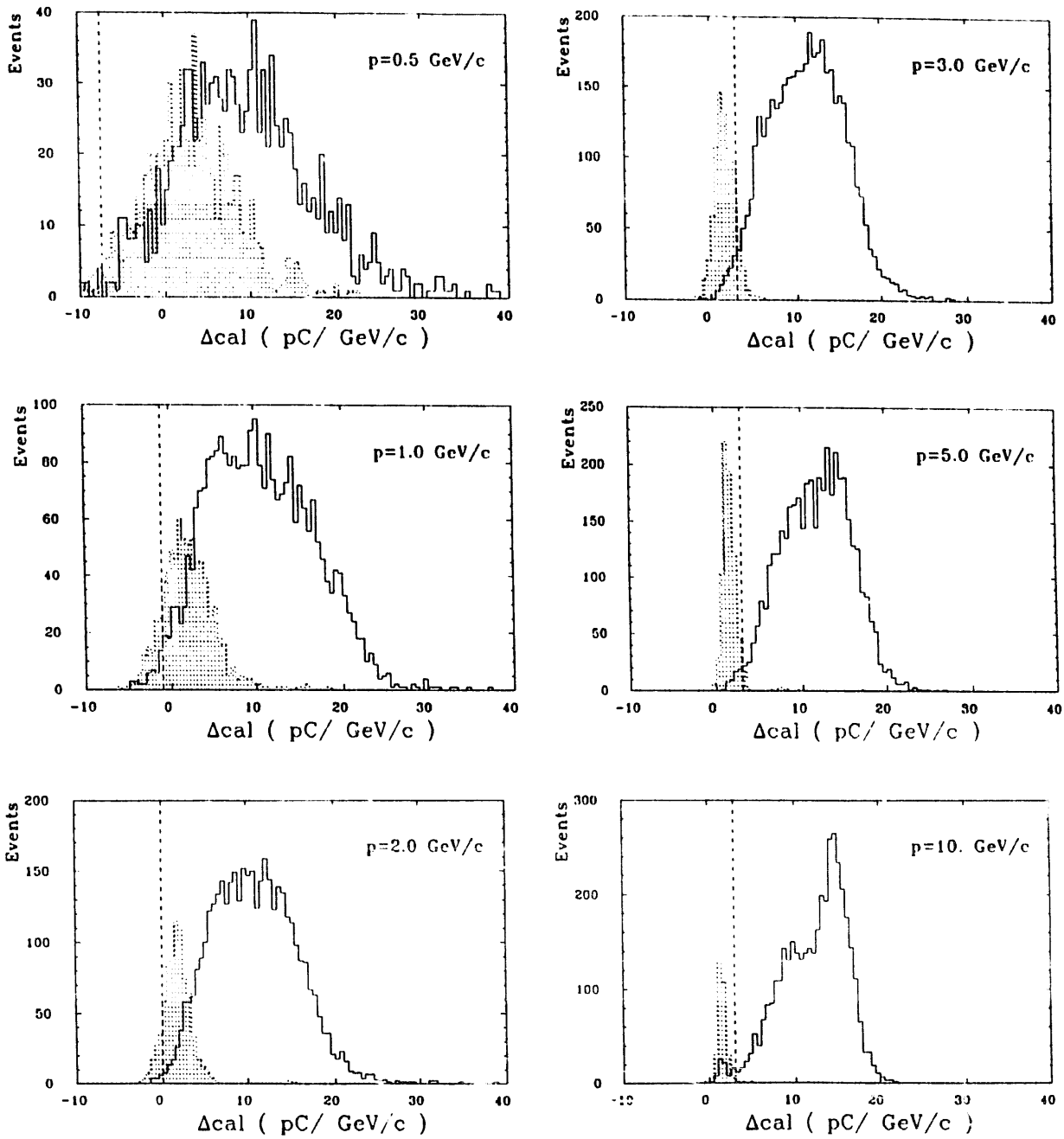

Fig. 9. Δ_{cal} spectra for electrons and hadrons at different beam momenta. The electron distribution is filled with dots and the value of Δ_{cut} used to reject electrons is indicated with a dashed line. The electron and hadron samples have been selected using the Cherenkov counters.

for all beam momenta. The contamination of these samples is discussed in the next section.

7. Beam composition, selection criteria and background

The beam used in this test was produced by 24 GeV/c protons impacting on a 7 cm long tungsten target. This target was located about 30 m upstream of the calorimeter. The beam composition * is reported in table 4. At low momenta the beam was dominated by electrons and positrons, whereas at high momenta hadrons, especially protons, were dominant.

The hadron content of the beam was estimated using the cross-sections given in ref. [7]. The predicted frac-

* The pion samples contain about 5% muons.

Table 3
Electron rejection $r_{cal}(e)$ achieved with the calorimeter cut $\Delta_{cal} > \Delta_{cut}$. The hadron efficiency of this cut, $\epsilon_{cal}(h)$, is also shown

p [GeV/c]	Δ_{cut} [pC/GeV]	$r_{cal}(e)$ [%]	$\epsilon_{cal}(h)$ [%]
0.50	−7.5	1.2	99.3
0.75	−5.0	1.9	99.4
1.00	−2.5	5.3	99.4
1.50	−1.0	6.5	99.7
2.00	0.0	12.0	99.6
3.00	3.0	89.8	97.9
5.00	3.0	96.2	99.0
7.00	3.0	99.0	98.6
10.00	3.0	99.0	99.0

tions of protons and pions are in qualitative agreement with the measured ones. The predicted fractions of kaons and antiprotons are reported in table 5 and will be used for background estimates. The decays of pions and kaons in the beamline were taken into account. The decay in flight probability is

$$r = 1 - \exp\left(-\frac{L_b}{pd}\right),$$

where $L_b = 30$ m and d is the decay length (56 m (GeV/c)$^{-1}$ for pions and 7 m (GeV/c)$^{-1}$ for kaons). The factor r for pions and kaons is also shown in table 5. The absence of kaons at low momenta is explained by this decay factor. We observe that for $p \geq 3$ GeV/c, about 2% of the hadron beam was due to kaons and antiprotons. This value is in agreement with the observed number of particles tagged as "protons" by the Cherenkov counters for the negative polarity of the beam.

An energy scan was performed with the beam incident on the centre of EMC section 7 in module 2 (see fig. 1) in the momentum range of 0.5 to 10 GeV/c. The data were taken for both beam polarities and, above 3 GeV/c, for the two values of the Cherenkov pressure mentioned in section 6. The particle selection criteria are summarized below

Table 4
Beam composition

p [GeV/c]	f_{e^+} [%]	f_{e^-} [%]	f_{π^+} [%]	f_{π^-} [%]	f_p [%]
0.50	44.6	45.5	4.7	4.6	0.5
1.00	39.8	44.1	6.5	7.1	2.5
1.50	36.5	33.9	12.0	11.8	5.9
2.00	27.2	30.2	16.9	17.6	8.1
3.00	17.5	16.7	30.0	23.7	12.0
5.00	6.1	5.6	40.2	24.9	23.2
7.00	2.1	1.6	36.8	20.4	39.0
10.0	0.3	0.2	27.3	11.7	60.5

- Electrons: a signal above threshold was required in both Cherenkov counters, C1 and C2 (pressure pr_1), and an additional cut was applied in Δ_{cal} (see section 6).
- Pions: it was required, no signal in the Cherenkov counters (pressure pr_1) for $p < 3$ GeV/c, but a signal above threshold (pressure pr_2) for $p \geq 3$ GeV/c. The calorimeter cut $\Delta_{cal} > \Delta_{cut}$ was used for all beam momenta. In addition, a TOF measurement compatible with pions for $p < 3$ GeV/c was required. A simple shower topology cut using the correlated signal in the HAC1 and HAC2 sections was used to reject muons.
- Protons: for $p < 3$ GeV/c, a TOF measurement compatible with protons was required. For $p \geq 3$ GeV/c, no signal in the Cherenkov counters (pressure pr_2) was demanded, in addition to the calorimeter cut $\Delta_{cal} > \Delta_{cut}$.

We estimate the contamination of the electron sample after cuts to be about 0.1%. The pion sample is contaminated by electrons. This contamination was calculated from the efficiency of the Cherenkov counters and calorimeter cut:

$$\frac{n_e}{n_\pi} = (1 - \epsilon_1(pr_1))(1 - \epsilon_2(pr_1))(1 - r_{cal}(e))\frac{f_e}{f_\pi}$$

for $p < 3$ GeV/c,

$$\frac{n_e}{n_\pi} = (1 - r_{cal}(e))\frac{f_e}{f_\pi} \quad \text{for} \quad p \geq 3 \text{ GeV}/c,$$

Table 5
Kaon and antiproton content of the beam, relative to protons and pions, as predicted by the model of ref. [7]. The decay probabilities in the beamline of pions and kaons, r_π and r_K are also indicated

p [GeV/c]	r_π	r_K	K^+/π^+ [%]	K^+/p [%]	K^-/π^- [%]	$\bar{p}/\pi^-$ [%]	$(K^- + \bar{p})/\pi^-$ [%]
1.00	0.41	0.99	–	0.3	–	–	–
2.00	0.23	0.88	0.9	3.7	0.4	–	0.4
3.00	0.16	0.76	2.0	6.1	1.1	0.1	1.2
5.00	0.10	0.58	3.9	6.3	1.9	0.2	2.1
7.00	0.07	0.46	5.2	5.2	1.9	0.3	2.2
10.00	0.05	0.35	8.3	3.3	1.3	0.2	1.5

Table 6
Contamination of pion and proton samples. The contamination of pions by electrons and of protons by pions are calculations taking into account the efficiency of the Cherenkov counters. The contamination of protons by kaons is a prediction obtained from the theoretical model of ref. [7]

p [GeV/c]	n_{e^+}/n_{π^+} [%]	n_{e^-}/n_{π^-} [%]	n_{π^+}/n_p [%]	n_{K^+}/n_p [%]
0.50	9.4	9.8	–	–
0.75	6.8	6.8	–	–
1.00	4.0	4.1	–	–
1.50	2.0	1.9	–	–
2.00	0.9	1.0	–	–
3.00	5.8	7.0	2.5	(6.1)
5.00	0.6	0.9	0.1	(6.3)
7.00	0.1	0.1	–	(5.2)
10.00	–	–	–	(3.3)

where ϵ_1 and ϵ_2 are the Cherenkov efficiencies, r_{cal} the calorimeter cut efficiency for electron rejection and f_e, f_π are particle fractions (see tables 2, 3 and 4). The contamination values calculated for both beam polarities are given in table 6. The contamination of the proton sample is about 0.1% below 3 GeV/c. Above this value, the proton sample is contaminated by pions and kaons. The contamination by pions is

$$\frac{n_\pi}{n_p} = (1-\epsilon_1(pr_2))(1-\epsilon_2(pr_2))\frac{f_\pi}{f_p}.$$

The contamination by kaons, n_K/n_p, was obtained from the predicted values of table 5. A summary of the contamination estimates for the proton sample is also included in table 6.

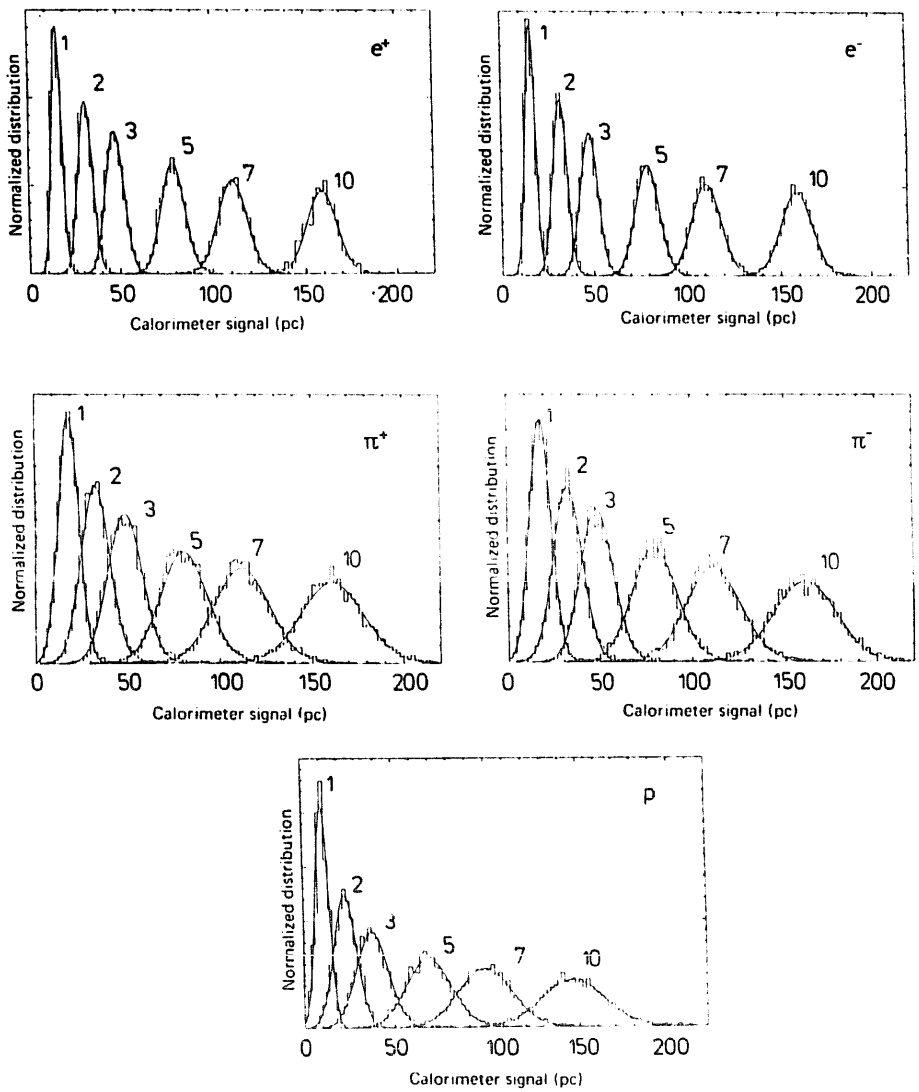

Fig. 10. Pulse-height distributions for e^+, e^-, π^+, π^- and p of momenta from 1 to 10 GeV/c. All calorimeter channels have been summed up and Gaussian fits are overlayed. The distributions are normalized to the same number of events.

8. Energy resolution and e/h

The pulse-height distributions of electrons, pions and protons selected according to the criteria presented in section 7 are shown in fig. 10 for beam momenta of 1, 3, 5, 7 and 10 GeV/c. The pulse-height distributions for $p = 0.5$ GeV/c are also shown in fig. 11. These distributions were obtained by summing the charge deposited in all 144 calorimeter channels. We observe that all distributions are well represented by Gaussian functions even for the lowest momentum of 0.5 GeV/c.

The average values and fractional energy resolutions obtained from the Gaussian fits of all distributions are given in tables 7 and 8. The most relevant features contained in these tables are listed below.

(1) Electrons and positrons yield the same calorimeter response within statistical errors (see fig. 12a). This response is also linear with deviations δ smaller than 1% (see table 7) except for the lowest momentum (0.5 GeV/c) where the sensitivity to small pedestal shifts is significant. These results are in agreement with Monte Carlo calculations performed with the EGS4 Monte Carlo generator [8].

(2) The fractional energy resolution for electrons is $17.5\%/\sqrt{p}$ (only the response to three EMC sections, containing 99% of the deposited energy, is considered, see fig. 12b). This result is in agreement with previous measurements [5] and with EGS4 calculations assuming a contribution of about $9\%/\sqrt{E}$ from photoelectron statistics. If the response of the whole calorimeter is considered, the resolution is degraded at low energies due to a noise contribution of $15\%/p$ (see fig. 12b).

(3) Pions of both polarities give the same calorimeter response, at least down to beam momenta of 0.5 GeV/c (see fig. 13a). The e/π ratio is about 1 for $p \geq 3$ GeV/c but decreases significantly for lower momenta.

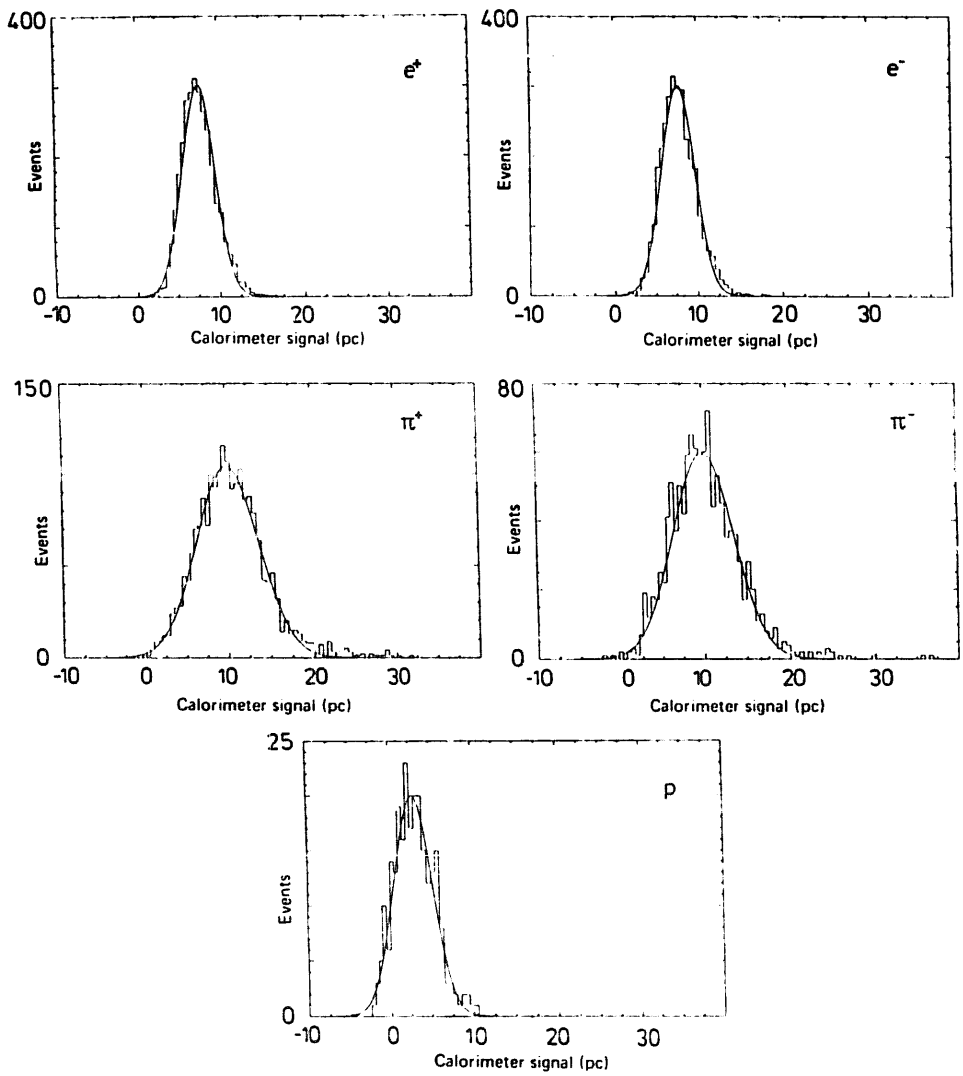

Fig. 11. Pulse-height distributions for e^+, e^+, π^+, π^- and p of 0.5 GeV/c momentum. All calorimeter channels have been summed up and Gaussian fits are overlayed.

Table 7
Average response and energy resolution for electrons

p [GeV/c]	$\langle E\rangle/p$ [pC/GeV] All sections	δ [%]	$(\sigma/\langle E\rangle)\sqrt{p}$ [%] All sections	$(\sigma/\langle E\rangle)\sqrt{p}$ [%] 3 EMC sections only
+0.50	16.40±0.12	+1.6	27.4±0.3	18.4±0.2
+0.75	16.20±0.08	+0.4	24.3±0.4	17.4±0.2
+1.00	16.00±0.07	−0.8	23.1±0.3	17.5±0.2
+1.50	15.93±0.05	−1.3	22.0±0.3	18.1±0.2
+2.00	16.04±0.04	−0.6	19.4±0.2	16.4±0.2
+3.00	16.18±0.03	+0.3	19.9±0.3	17.9±0.2
+5.00	16.16±0.03	+0.1	18.9±0.3	17.9±0.2
+7.00	16.15±0.02	+0.0	18.9±0.3	17.9±0.3
+10.0	16.17±0.04	+0.2	17.6±0.6	16.5±0.5
−0.50	16.50±0.12	+2.3	27.3±0.3	18.4±0.2
−0.75	16.11±0.08	+0.0	24.4±0.3	17.9±0.2
−1.00	15.98±0.06	−0.8	23.4±0.3	17.2±0.2
−1.50	16.07±0.05	−0.3	21.4±0.3	17.3±0.2
−2.00	16.08±0.04	−0.2	19.4±0.3	17.4±0.2
−3.00	16.16±0.03	+0.2	20.0±0.3	17.9±0.2
−5.00	16.23±0.02	+0.7	18.5±0.3	17.9±0.2
−7.00	16.17±0.02	+0.3	18.4±0.3	18.2±0.2
−10.0	16.17±0.02	+0.3	17.2±0.4	16.6±0.3

The fractional energy resolution is also similar for both polarities and about $34\%/\sqrt{p}$ for $p \geq 2$ Gev/c, with a significant decrease at low momenta (see fig. 13b). These results are also consistent with previous measurements [5].

(4) The e/h ratio and the fractional energy resolution are very different for protons and pions, when evaluated at the same beam momentum (see fig. 13a and b), but are similar when evaluated at the same kinetic energy (see fig. 14a and b).

The response of the calorimeter at low energies shown in fig. 14a can be qualitatively understood: since the interaction length for pions is 1.2λ and dE/dx losses for minimum ionizing particles (mips) are 200 MeV/λ [9], pions with kinetic energies below 250 MeV lose their energy almost completely by ionization before undergoing any hadronic interaction. This effect is further increased if the dE/dx low β rise, which starts below 200 MeV (see fig. 15 and ref. [10]), is taken into account. Therefore a ratio

$$\frac{e}{\pi} \sim \frac{e}{\text{mip}}$$

is expected below a kinetic energy of about 300 MeV. The e/mip value is 0.62 according to EGS4 calculations. This effect occurs both for pions and protons.

As commented in section 3, dE/dx losses in the matter located in front of the calorimeter must be taken into account at very low momenta. They represent only about 3% of the total kinetic energy for $p = 1$ GeV/c protons but 20% for $p = 0.5$ GeV/c protons. The e/h

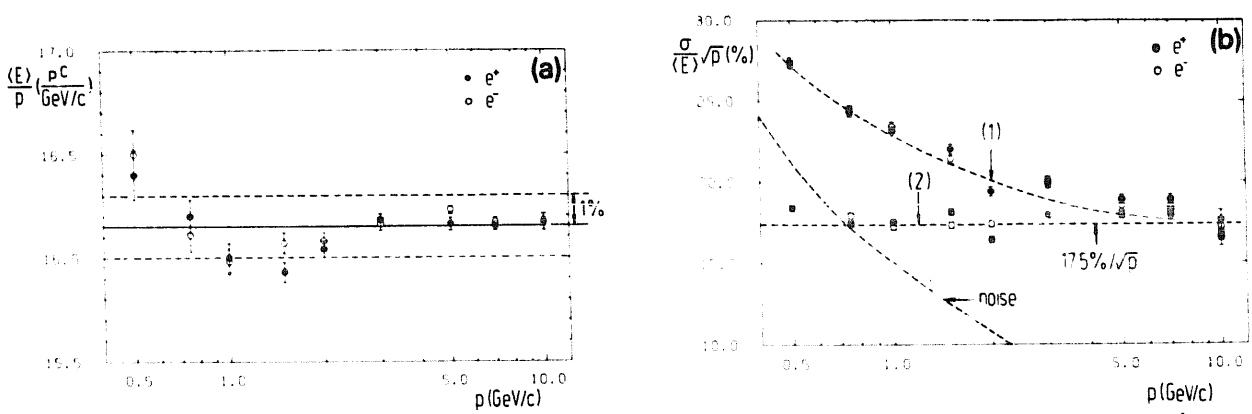

Fig. 12. (a) Linearity of the electron response. (b) Energy resolution for electrons (1) with all calorimeter sections summed up and (2) with only three EMC sections summed up. The total calorimeter noise is indicated.

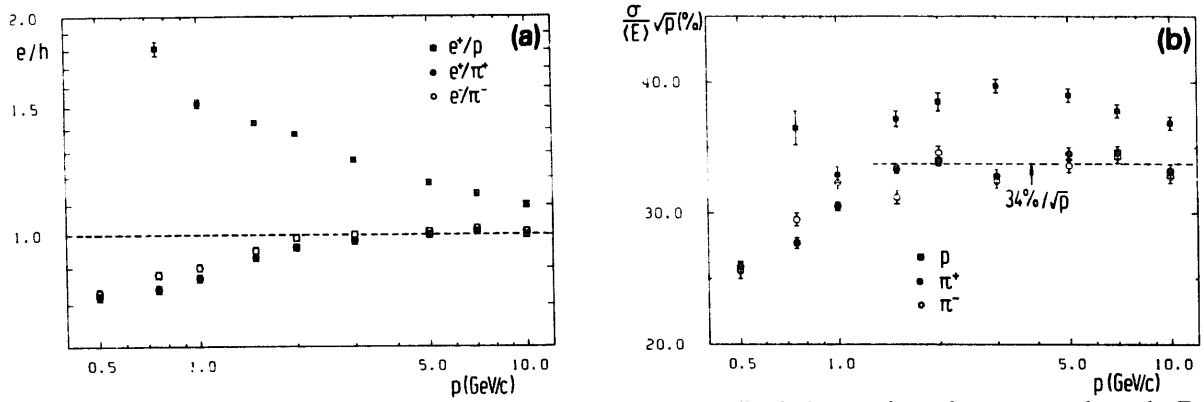

Fig. 13. (a) e/h as a function of the beam momentum for protons and pions. All calorimeter channels are summed up. (b) Energy resolution for hadrons as a function of the beam momentum. All calorimeter channels are summed up.

Table 8
e/h ratios and energy resolution for pions and photons

p [GeV/c]	e/π	e/p	$(\sigma/\langle E\rangle)\sqrt{p}$ Pions [%]	$(\sigma/\langle E\rangle)\sqrt{p}$ Protons [%]
+0.50	0.82±0.01	2.90±0.16	25.9±0.4	58.2±3.2
+0.75	0.84±0.01	1.81±0.04	27.7±0.4	36.5±1.3
+1.00	0.87±0.01	1.52±0.02	30.5±0.3	32.9±0.6
+1.50	0.93±0.01	1.43±0.01	33.3±0.3	37.2±0.6
+2.00	0.96±0.01	1.38±0.01	33.9±0.3	38.5±0.7
+3.00	0.98±0.01	1.27±0.01	32.8±0.5	39.7±0.5
+5.00	1.00±0.01	1.18±0.01	34.5±0.5	39.0±0.5
+7.00	1.01±0.01	1.14±0.01	34.6±0.5	37.8±0.5
+10.0	1.00±0.01	1.10±0.01	33.2±0.5	36.9±0.5
−0.50	0.83±0.01		25.6±0.6	
−0.75	0.88±0.01		29.5±0.5	
−1.00	0.90±0.01		32.3±0.5	
−1.50	0.95±0.01		31.2±0.5	
−2.00	0.99±0.01		34.6±0.5	
−3.00	1.00±0.01		32.4±0.5	
−5.00	1.01±0.01		33.6±0.5	
−7.00	1.02±0.01		34.3±0.5	
−10.0	1.01±0.01		32.8±0.5	

values before and after correction for these energy losses are shown as a function of kinetic energy in tables 9a and 9b. The values displayed in fig. 14a are the corrected ones.

We note finally that the shift in e/π and e/p due to contamination of the hadron samples by electrons and kaons is very small (see table 10), typically below 1%. We estimate the total systematic error of our measurements to be about 2%. This value includes calibration errors and uncertainties in the contamination of the event samples.

The energy fractions deposited in the different calorimeter sections (EMC, HAC1, HAC2) by protons and pions of both polarities are given in table 11 and fig. 16 versus beam momentum. The energy deposition of protons and pions are very similar for beam momenta above 2 GeV/c. Below this value, the dE/dx rises for protons (see fig. 15) and therefore all the energy is absorbed in the EMC sections by ionization.

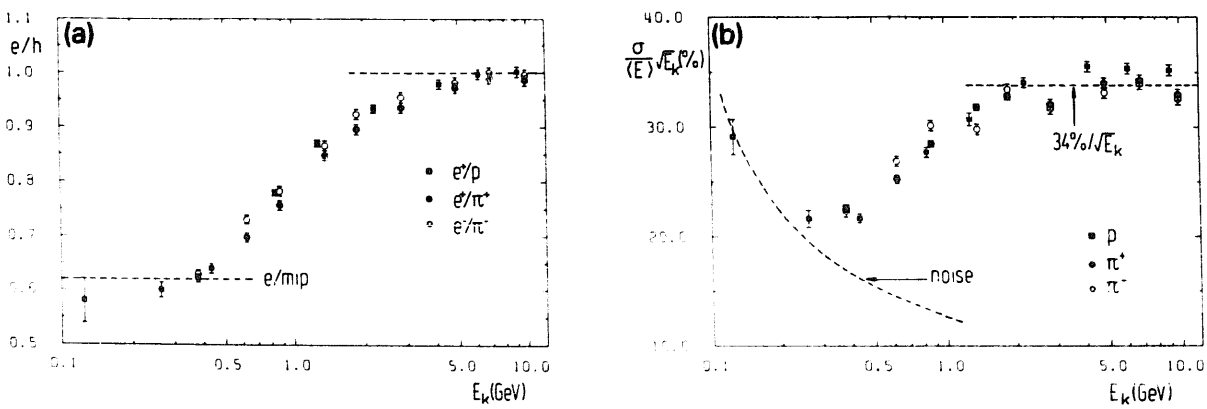

Fig. 14. (a) e/h as a function of the kinetic energy for protons and pions. The electron values have been scaled assuming a perfect linearity of the calorimeter response and the hadron values have been corrected for energy losses in front of the calorimeter. (b) Energy resolution for hadrons as a function of the kinetic energy. The total calorimeter noise is indicated.

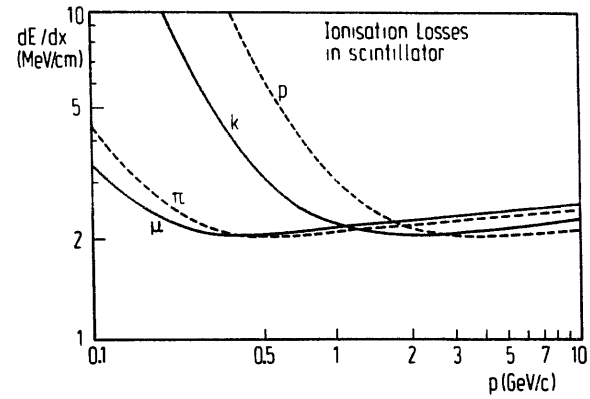

Fig. 15. dE/dx losses in scintillator as a function of particle momentum for μ, π, K and p.

9. Summary

We have measured the response of a sandwich calorimeter, consisting of 3.3 mm thick uranium plates interleaved with 2.6 mm thick scintillator tiles, to electrons, pions and protons in the momentum range of 0.5 to 10 GeV/c. We have found the following results:
(1) the electron response is linear within 1% in the

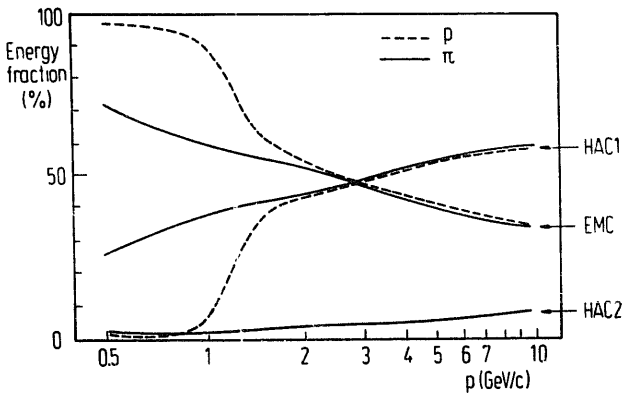

Fig. 16. Energy deposition by protons and pions in the different calorimeter sections as a function of the beam momentum.

Table 9
e/h ratio for positive pions (a) and for protons (b) as a function of kinetic energy before and after correcting for energy losses in front of the calorimeter

E_k [GeV]	e/π measured	e/π corrected	(a)
0.38	0.62±0.01	0.61±0.01	
0.62	0.70±0.01	0.69±0.01	
0.87	0.76±0.01	0.75±0.01	
1.37	0.85±0.01	0.85±0.01	
1.86	0.90±0.01	0.90±0.01	
2.86	0.94±0.01	0.94±0.01	
4.86	0.97±0.01	0.97±0.01	
6.86	0.99±0.01	0.99±0.01	
9.86	0.99±0.01	0.99±0.01	
	e/p measured	e/p corrected	(b)
0.12	0.72±0.04	0.58±0.04	
0.26	0.63±0.01	0.60±0.01	
0.43	0.66±0.01	0.64±0.01	
0.83	0.79±0.01	0.78±0.01	
1.27	0.88±0.01	0.87±0.01	
2.21	0.93±0.01	0.93±0.01	
4.15	0.98±0.01	0.98±0.01	
6.12	1.00±0.01	1.00±0.01	
9.11	1.00±0.01	1.00±0.01	

Table 10
Shift in e/π and e/p due to contamination

p [GeV/c]	$\delta(e/\pi)$ [%]	$\sigma(e/p)$ [%]
0.50	−1.7	-
0.75	−1.1	-
1.50	−0.5	-
1.00	−0.1	-
2.00	−0.4	-
3.00	−0.1	+1.2
5.00	-	+0.6
7.00	-	+0.4
10.00	-	+0.2

Table 11
Fraction of energy deposited in the different calorimeter sections

p [GeV/c] section	f_{π^+} [%]			f_{π^-} [%]			f_p [%]		
	EMC	HAC1	HAC2	EMC	HAC1	HAC2	EMC	HAC1	HAC2
0.50	71.7	26.2	2.1	73.4	24.7	1.9	96.0	3.0	1.0
0.75	64.2	34.9	0.8	63.9	34.9	1.2	95.4	4.2	0.4
1.00	59.7	38.8	1.5	60.0	38.7	1.3	92.1	4.4	3.4
1.50	55.5	41.5	3.0	56.0	41.3	1.7	61.0	37.7	1.3
2.00	53.5	43.7	2.8	54.8	42.2	2.7	54.1	43.9	2.0
3.00	46.0	51.4	2.6	44.4	52.6	3.0	47.6	49.8	2.6
5.00	40.1	55.1	4.8	40.7	54.7	4.6	40.6	54.1	5.4
7.00	36.4	57.2	6.4	36.8	57.2	6.0	36.7	56.7	6.6
10.0	32.9	59.2	7.9	32.1	59.8	8.1	33.5	58.9	7.6

momentum range considered and there is no significant difference between the response of e^+ and e^-;
(2) the energy resolution for electrons is $17.5\%/\sqrt{p}$ over the whole momentum range;
(3) the response for π^+ and π^- is similar down to 0.5 GeV/c. The e/π ratio approaches 1 for $p \geq 3$ GeV/c and the e/mip value of 0.62 at the lowest momenta;
(4) the energy resolution for pions is $34\%/\sqrt{p}$ for $p \geq 2$ GeV/c with some improvement at lower momenta;
(5) protons give the same response as pions for the same value of the kinetic energy.

These results are in good agreement with those published in ref. [2].

Acknowledgements

We gratefully acknowledge the support of the technical staff from the collaboration institutes for the installation and transport of the calorimeter. We are indebted to our colleagues from York University for the construction of the modules and from Nevis and ANL for providing the analog and digital cards used in the test. We want to thank all our colleagues from the ZEUS collaboration who helped to carry out the measurements or to perform the data analysis. We are grateful for the hospitality of CERN and for the support of the CERN technical staff during the measurements.

References

[1] ZEUS, a detector for HERA, Letter of Intent, DESY (June 1985); The ZEUS detector, Technical Proposal, DESY (March 1986); The ZEUS detector, Status Report 1987, DESY (Sept. 1987); The ZEUS detector, Status Report 1989, DESY (March 1989).
[2] T. Akesson et al., Nucl. Instr. and Meth. A241 (1985) 17.
[3] B. Anders et al., DESY 86-105 (Sept. 86);
G. d'Agostini et al., Nucl. Instr. and Meth. A274 (1989) 134;
T. Akesson et al., Nucl. Instr. and Meth. A262 (1987) 243.
[4] H. Brückmann, Hadron calorimetry – a puzzle of physics, Proc. Workshop on Compensated Calorimetry, Pasadena (1985) CALT-68-1305;
R. Wigmans, Nucl. Instr. and Meth. A259 (1987) 389.
[5] U. Behrens et al., DESY 89-128 (1989).
[6] W. Buttler et al., Nucl. Instr. and Meth. A277 (1989) 217;
B. Sippach et al., Development of the front end electronics for the ZEUS calorimeter, contribution to the IEEE Symp., Orlando, Florida (1988);
A. Caldwell et al., Implementation of a high precision readout system for the ZEUS calorimeter, to be published.
[7] H. Grote, R. Hagedorn and J. Ranft, Atlas of particle production spectra, CERN (1970).
[8] W.R. Nelson, H. Hirayama and D.O. Rogers, SLAC-265 (1985).
[9] Particle Data Group, Review of particle properties, Phys. Lett. B204 (1988).
[10] W. Lohmann, R. Kopp and R. Voss, CERN 85-03 (1985).